

# Numerical Study of Flow Over Annular-Finned Tube Heat Exchangers by Different Turbulent Models

Hossain Nemati<sup>c</sup> and Mohammad Moghimi

*Faculty of Mechanical Engineering, Islamic Azad University, Marvdasht branch  
Marvdasht, IRAN*

Received: 20/01/2014 – Revised 14/07/2014 – Accepted 17/08/2014

## Abstract

In the present study, turbulent flow passing over a four-row finned tube heat exchanger has been simulated by nine different turbulent models. Annular fin has a complex geometry and as a result, very complex phenomena such as flow separation, horseshoe vortices, generated wakes, etc. may be observed. Results have been compared with experimental correlations and in more detail to each other. In addition, capability of numerical models as a flow visualization tool, their strengths and weaknesses have been studied.

*Keywords: Annular fins; Fin tube; turbulent flow; turbulent models; Staggered.*

## 1. Introduction

The optimization design of heat exchangers depends directly not only on knowing global heat transfer and pressure drop, but also on the clear understanding of flow and heat transfer through a complex geometry of finned-tube bank. So, it is very vital to know fluid behavior and its tradeoffs between heat transfer, fluid flow and finned-tube surface area. Although average heat transfer coefficient data are needed to calculate the finned-tube performance, a deep understanding of the local heat transfer behavior improves fin performance. Unfortunately, complexity of finned-tube geometry makes it difficult to have a clear understanding of fluid flow pattern. Generally, there are three main methods in simulating or visualizing the fluid flow, passing through the finned-tube, experimentally. These methods are total heating, point heating, and mass transfer methods. In total heating method, the entire surface of the fin is heated by a flux through the fin base and then temperatures and heat fluxes is measured locally on the fin surface. Although thermal boundary conditions at the fin surface in this method are very realistic, the intrusion of measuring tools into the fluid flow and the heat conduction paths inside the fin is the main disadvantage of this technique. Furthermore, the impact of such intrusions is not clear. This method has been in determination of local heat transfer coefficient [1, 2]. On the other technique, the point heating method, a uniform flux is providing through a small strip on the surface of the fin; then, fin surface temperature is measured by placing thermocouples on fin surface and as a result, local flux and measured temperature determine the local heat transfer coefficient. However, thermal boundary conditions in this method are completely unrealistic, so, its results are accompanied with serious errors. Raised errors in this method have been mentioned in work of Stasiulevicius and Skrinska [3]. The last method is mass transfer methods, in which a similarity between heat and mass transfer is used to estimate local heat transfer coefficient. To do this, the entire surface of a specimen should

<sup>c</sup> Corresponding Author: Hossain Nemati

Email: [Nemati.hossain@gmail.com](mailto:Nemati.hossain@gmail.com)

© 2014 All rights reserved. ISSR Journals

be coated with a substance which sublimates easily into the flow. Hu [4] performed this method on a single row tube bank with annular fin. She estimated local *Sherwood* number distributions for *Reynolds* number in range, 3000 to 12,000. Difficulties of this method prevent researchers to use it for multi row tube bank.

As it is clear, above mentioned methods are not so efficient and useful in describing the local behavior of fluid flow and heat transfer. Among all types of fins, annular fins have a special place. The severe complex geometry of this type makes the flow pattern more complex and also more interesting. Although numerous correlations can be found in literature to predicate total *Nusselt* number for annular fins, as it was asserted correctly by Xi and Torikoshi [4] "...experimental studies cannot adequately reveal the flow and thermal characteristics in finned-tube heat exchangers." Therefore, to provide better understanding about the most important heat transfer phenomena in flow passing annular finned-tube; computational fluid dynamics (CFD) technique may be very helpful. Especially, one can visualize detailed flow structures as well as temperature distribution by means of numerical simulation. Some numerical investigations have been performed for plate-finned tube bundles [5-9]; however, nothing may be found for annular finned tube. The first numerical work on annular finned tube was performed by Jang *et al* [10]. They studied numerically and experimentally fluid flow and heat transfer performance in a four row annular finned tube heat exchangers, assuming laminar flow regime. Their work then was followed by Mon and Gross considering turbulent flow regime [11].

In spite of all abilities and capacities of numerical method, it has its own difficulties and uncertainties. For example, the flow regime should be defined if it is laminar or turbulence. Normally the nature of the flow can be determined based on its *Reynolds* number. However, the main question is the type of flow in a circular finned-tube bank. Zhukauskas [12] solely stated that for circular finned-tube bundle, the critical value is  $Re = 10^5$ . However, Jacobi and Shah [13] argued that air flow may exhibit all of possible flow features (e.g., steady or unsteady, laminar or turbulent) in a single heat exchanger. Moreover, assuming turbulent flow regime, there are several models to simulate turbulent flow and the most economical or the best one is not clear. So, before using the numerical technique the above mentioned ambiguities should be clear. The purpose of this study is to compare results of some different turbulent models for a specified geometry and condition. For this reason, one fin geometry of those mentioned in [11] was used different turbulent models were performed and the results were compared in detail. The commercial computational fluid dynamics software package FLUENT was used to simulate the problem.

## 2. Numerical simulation

### 2.1. Geometry

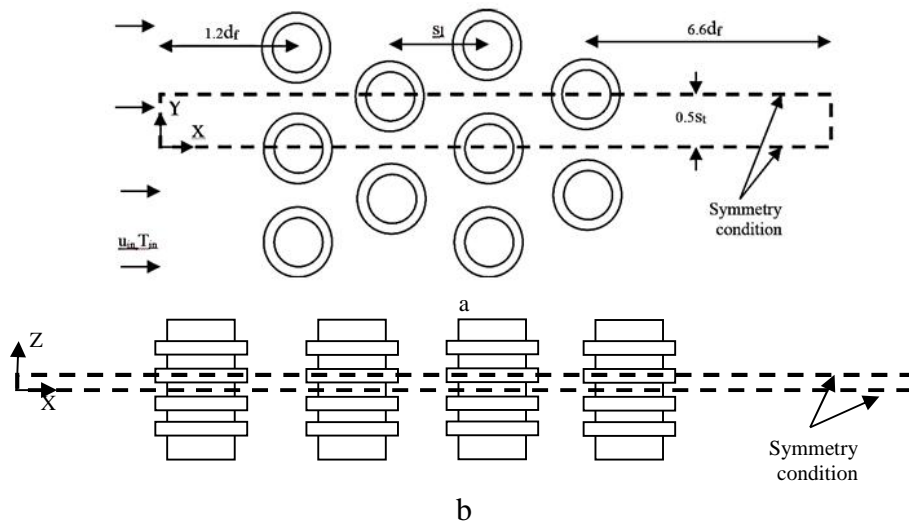
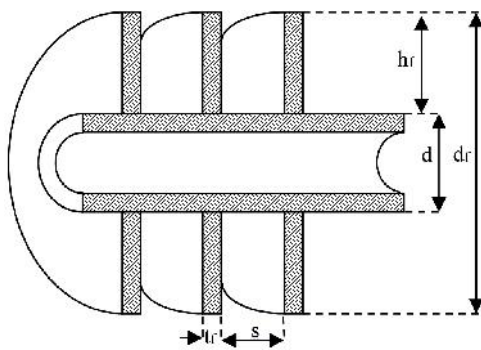


Figure 1. Schematic view of the simulated finned-tube bundle.

A schematic view of the simulated finned-tube bundle has been proposed in Figure 1. The assumed geometry comprises four rows finned-tube bundle, where due to flow and geometry symmetry, it can be reduced to the zone surrounded by dotted lines. Also, cross section of annular finned-tube is shown in Figure 2.



Fin			
diameter	height	thickness	spacing
$d_f$	$h_f$	$t_f$	$s$
34	5	0.5	2
Tube		Tube Pitch	
Outside Diameter	Transverse	Longitudinal	
$d$	$S_t$	$S_l$	
24	40.8	35.33	

Figure 2. cross section of annular finned-tube

## 2.2. Governing equations

For steady flow through the tube bank, momentum equation is:

$$\dots \frac{\partial}{\partial x_j} (u_i u_j) = -\frac{\partial P}{\partial x_j} + \frac{\partial}{\partial x_j} \left[ \sim \left( \frac{\partial u_i}{\partial x_j} + \frac{\partial u_j}{\partial x_i} - \frac{2}{3} u_{ij} \frac{\partial u_l}{\partial x_l} \right) \right] + \frac{\partial}{\partial x_j} (-\overline{u'_i u'_j}) \quad (1)$$

where the last term in right side of Eq. 1 is applicable whenever the flow is turbulent. It is an unfortunate fact that no single turbulent model has been universally accepted as being superior for all classes of problems [14]. Several models are available to model these Reynolds stresses,  $-\overline{u'_i u'_j}$ , in order to close Eq. 1. A common method employs the Boussinesq hypothesis to relate the Reynolds stresses to the mean velocity gradients:

$$-\overline{u'_i u'_j} = \sim_t \left( \frac{\partial u_i}{\partial x_j} + \frac{\partial u_j}{\partial x_i} \right) - \frac{2}{3} \left( \dots k + \sim_t \frac{\partial u_l}{\partial x_l} \right) u_{ij} \quad (2)$$

Based on Boussinesq hypothesis, several models are developed to simulate Reynolds stresses. In the following a brief description of each model including strengths and weaknesses are presented. The relative equations and details of theories are omitted for brevity's sake. The readers may consult FLUENT manual [14].

### ➤ *Spalart-Allmaras model- Standard, Modified* (one equation model)

The Spalart-Allmaras model is a one-equation model that solves a modeled transport equation for the turbulent viscosity,  $\sim_t$ . The Spalart-Allmaras model has been designed specifically for aerospace applications involving wall-bounded flows and has been shown to give good results for boundary layers subjected to adverse pressure gradients. However, it has not been calibrated for general industrial flows and may produce relatively larger errors for some free shear flows, especially plane and round jet flows. In addition, it cannot be relied on, to predict the decay of homogeneous, isotropic turbulence. There is a modified version of this model in FLUENT. This modification considers the effect of combination of both vorticity and strain tensors simultaneously.

### ➤ *k- models- Standard, RNG, Realizable* (two equation model)

k- models are categorized in two-equation models in which, both turbulent length and time scale are determined by solving two separate transport equations. Three different version of k- models are found in FLUENT. The standard k- model is the most common model in simulating turbulent flow. Robustness, economy, and reasonable accuracy for a wide range of turbulent flows explain its popularity in industrial flow and heat transfer

simulations. It is a semi-empirical model, and the derivation of the model equations relies on phenomenological considerations and empiricism. The draw-back of all  $k$ - models is their insensitivity to adverse pressure gradients and boundary layer separation. They typically predict a delayed and reduced separation relative to observations. This can result in overly optimistic design evaluations for flows which separate from smooth surfaces (aerodynamic bodies, diffusers, etc.). The  $k$ - model is therefore not widely used in external aerodynamics.

The RNG  $k$ - model was derived using a statistical technique. It is similar in form to the standard  $k$ - model, but includes the following refinements:

- The RNG model has an additional term in its equation that improves the accuracy for rapidly strained flows.
- The effect of swirl on turbulence is included in the RNG model, enhancing accuracy for swirling flows.
- The RNG theory provides an analytical formula for turbulent Prandtl numbers, while the standard model uses pre-specified, constant values.
- While the standard model is a high-Reynolds-number model, the RNG theory provides an analytically-derived differential formula for effective viscosity that accounts for low-Reynolds-number effects.

These features make the RNG  $k$ - model more accurate and reliable for a wider class of flows than the standard model.

The realizable  $k$ - model differs from the standard  $k$ - model in two important ways:

- The realizable  $k$ - model contains an alternative formulation for the turbulent viscosity.
- A modified transport equation for the dissipation rate,  $\epsilon$ , has been derived from an exact equation for the transport of the mean-square vorticity fluctuation.

The term “realizable” means that the model satisfies certain mathematical constraints on the Reynolds stresses, consistent with the physics of turbulent flows. Neither the standard  $k$ - model nor the RNG  $k$ - model is realizable. Both the realizable and RNG  $k$ - models have shown substantial improvements over the standard  $k$ - model where the flow features include strong streamline curvature, vortices, and rotation. Since the model is still relatively new, it is not clear in exactly which instances the realizable  $k$ - model consistently outperforms the RNG model. However, initial studies have shown that the realizable model provides the best performance of all  $k$ - model versions for several validations of separated flows and flows with complex secondary flow features.

➤ ***k*- models Standard, SST *k*-** (two equation model)

The standard  $k$ - model is an empirical model based on model transport equations for the turbulence kinetic energy ( $k$ ) and the specific dissipation rate ( $\epsilon$ ). The  $k$ - models are typically better in predicting adverse pressure gradient boundary layer flows and separation. The downside of the standard  $k$ -equation is a relatively strong sensitivity of the solution depending on the free stream values of  $k$  and  $\epsilon$  outside the shear layer. The use of the standard  $k$ - model is, for this reason, not generally popular.

The SST  $k$ - model (shear-stress transport) has been designed to avoid the free stream sensitivity of the standard  $k$ - model, by combining elements of the  $k$ -equation and the  $\epsilon$ -equation. In addition, the SST model has been calibrated to accurately compute flow separation from smooth surfaces. Within the  $k$ - model family, it is therefore recommended to use the SST model. It is typically somewhat more accurate in predicting the details of the wall boundary layer characteristics than the Spalart-Allmaras model.

➤ ***k-kl*- transition model** (three equation models)

The  $k$ - $kl$ - transition model [15] is used to predict boundary layer development and calculate transition onset. This model can be used to effectively address the transition of the boundary layer from a laminar to a turbulent regime. It is a relatively new method.

➤ **Transition SST model** (four equation models)

The transition SST model is based on the coupling of the SST  $kl$ - transport equations with two other transport equations, one for the intermittency and one for the

transition onset criteria, in terms of momentum-thickness Reynolds number. A FLUENT empirical correlation has been developed to cover standard bypass transition as well as flows in low free-stream turbulence environments.

### 2.3. Boundary conditions

Dry air enters normally to the computational domain with uniform velocity  $u_{in} = 2$  m/s, temperature  $T_{in} = 308.15$  K, turbulent intensity  $I=1\%$  and turbulent viscosity ratio equal to 2 (if required). No-slip boundary condition is assumed at the solid surfaces. Heat convection to the fin and heat conduction in the fin is considered. Solid material is assumed as aluminium. All tube surfaces including fins bases are assumed at constant temperature,  $T_w = 283.15$  K. At the symmetry planes, heat flux and normal velocity component are set to zero. Thermo-physical properties of air and aluminium are shown in Table 1.

Table 1: Thermo-physical properties of air and aluminium

	Density (kg/m <sup>3</sup> )	Conductivity (W/m.K)	Specific heat (J/Kg.K)	Viscosity (Kg/m.S)
Air	1.225	0.0242	1006.43	1.79E-05
Aluminium	2719	202.4	871	---

### 3. Solution strategy

Structured grid was generated to discretize domain. The basic grid included 95,760 cells. This amount of cells guarantees that  $y^+$  value nowhere exceeds 7. It then adapted for each method to reduce  $y^+$  value below 3. The generated grid in the central part of domain is shown in Figure 3. Nine different models described in previous section were used to determine heat transfer inside the domain. The laminar flow regime was considered through the fin space.

Defining  $\dot{H}$  as flow rate enthalpy, the amount of heat transfer from air to the fin,  $\dot{Q}$ , is calculated as:

$$\dot{Q} = \dot{H}_{out} - \dot{H}_{in} \quad (3)$$

Accordingly, heat transfer coefficient is defined as:

$$h = \frac{\dot{Q}}{(A - (1-y)A_f)_n} \quad (4)$$

in which  $A$  is total heat transfer area,  $A_f$  is fin surface area and  $n$  is log mean temperature difference,

$$n = \frac{T_{in} - T_{out}}{\ln(T_{in} - T_w) - \ln(T_{out} - T_w)} \quad (5)$$

Fin efficiency can be calculated iteratively by Eq. 6 and Eq. 7. [16]

$$y = \frac{\tanh(\mathbb{E}mh_f)}{\mathbb{E}mh_f} \left( 1 + .35 \ln \left( 1 + 2 \frac{h_f}{d} \right) \right) \quad (6)$$

$$m = \sqrt{2h/(k_f t_f)} \quad (7)$$

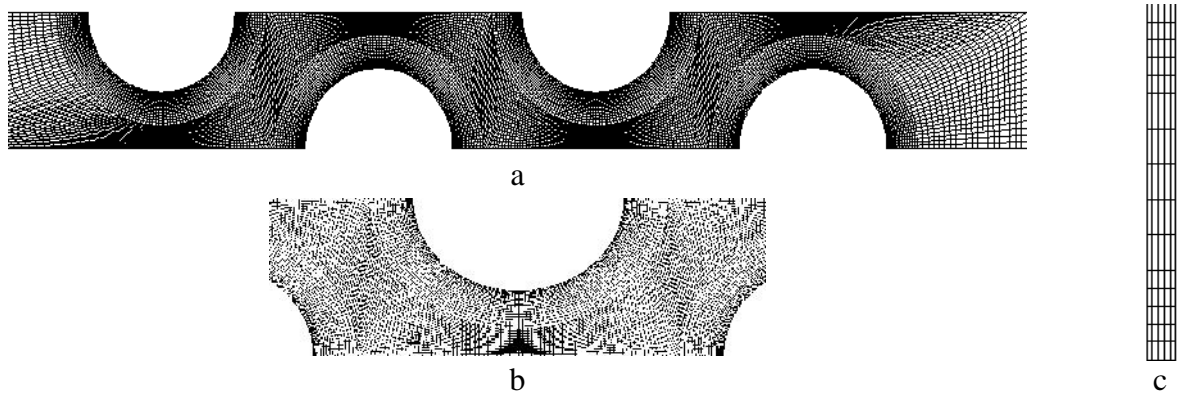


Figure 3. The generated grid in the central part of domain ( front view a and b - side view c)

#### 4. Results and discussion

##### 4.1. Heat transfer coefficient and pressure drop

The first step is comparing calculated global heat transfer in each method with experimental results. For this reason, mass weighted average outlet air temperature as well as pressure drop were calculated for each method. Accordingly, the following dimensionless parameters were calculated:

$$Nu = hd / k_f \quad (8)$$

$$Eu = \Delta P / \dots u_{\max}^2 \quad (9)$$

The Eq. 10 [17] and Eq. 11 [18] were used to compare with results of different models.

$$Nu = 0.38 Re^{0.6} Pr^{1/3} (A / A_t)^{-0.15}, \text{ (Ref. [17])} \quad (10)$$

$$Eu = 0.256 Re^{-0.264} (t_f / d_f)^{-0.377} (s / d)^{-0.396} (S_t / d)^{-0.396} n, \text{ (Ref. [18])} \quad (11)$$

The results are presented in Table 2.

Table 2: Numerical results

		$T_{out}$ (K)	$\dot{Q}$ (W)	$\Delta P$ (Pa)	$Eu$	$Nu$	$Nu$	$Eu$
Spalart- Allmaras	vorticity based	292.39	0.99	60.7	1.6	56.2		
	Strain vorticity	292.39	0.99	61.1	1.6	56.2		
k-	standard	292.11	1.01	80.2	2.2	57.9		
	RNG	292.07	1.01	72.3	1.9	58.2		
	Realized	292.03	1.01	62.5	1.7	58.5	60.4	1.8
k-	standard	292.23	1.00	55.8	1.5	57.2		
	SST	292.24	1.00	62.2	1.7	57.1		
K-Kl-	---	291.77	1.03	58.8	1.6	60.1		
Transition SST	---	292.02	1.01	65.5	1.8	58.5		

As it can be observed, the variation in outlet air temperature,  $T_{out}$ , is relatively small and calculated  $Nu$  shows good agreement with experimental results. However the estimated pressure drop is within a range from 55.8 Pa to 80.2 Pa. To investigate the reason of such discrepancy, in next section, the local behavior of flow in each method will be studied in detail.

##### 4.2. Local flow behaviour

Although the amount of calculated global heat transfer,  $q$ , is approximately the same, in all methods, the flow pattern, temperature contours and velocity distributions are not

exactly the same and they are different locally. So, in continue, the flow stream lines, velocity vector plot, temperature are compared.

First of all, flow stream lines in the symmetric plane between two adjacent fins are compared in each method shown in Figure4. As it can be observed, inside the tube bank; the flow field in all models is approximately the same. However, the length of predicted wake behind the last tube is totally different. In the k- family the results of all methods are approximately the same. However the RNG Method is more similar to standard method rather than realizable one. Interestingly, all, k-kl- Transition model, Transition SST model and Spalart-Allmaras models show a very good agreement with each other. However, they are slightly different from k- family. Unfortunately, all flow visualization methods are really inefficient and can not be used to judge.

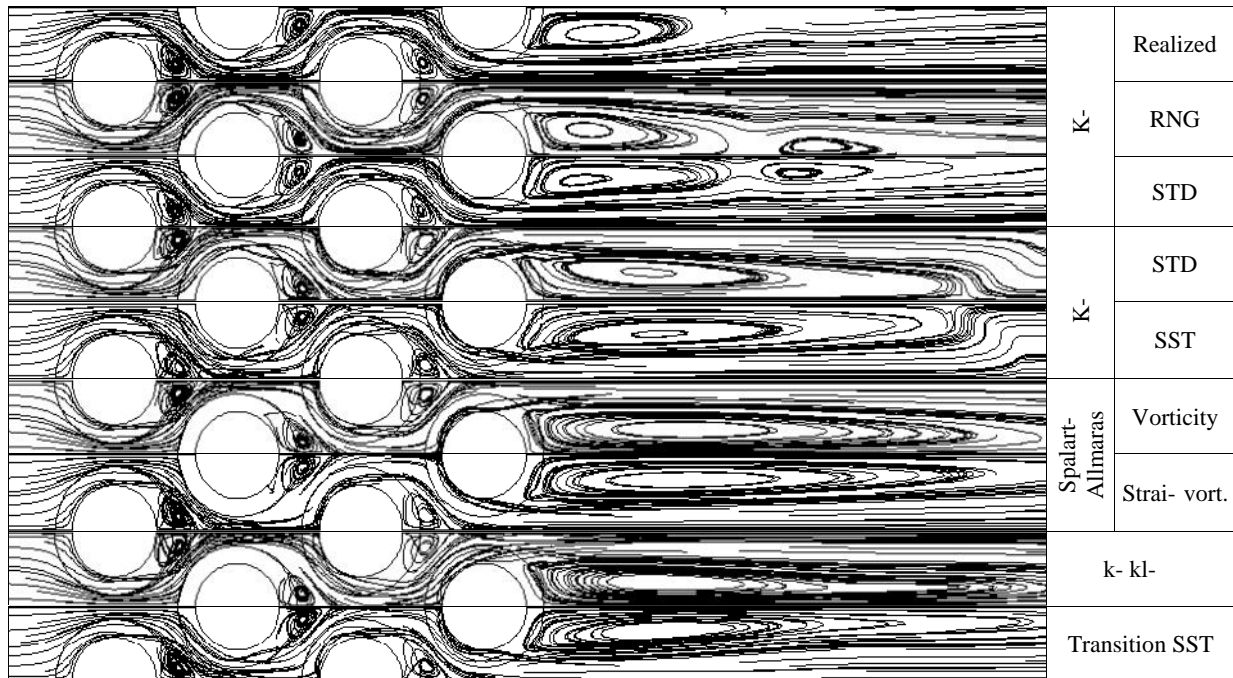


Figure 4. Flow pattern over tube in different models

The main phenomenon in heat transfer from fluid flow in finned tube bank is the flow separation. A schematic of general flow pattern over a second row of the staggered arrangement tube bundle presented by Neal and Hitchcock [1] is shown in Figure 5.

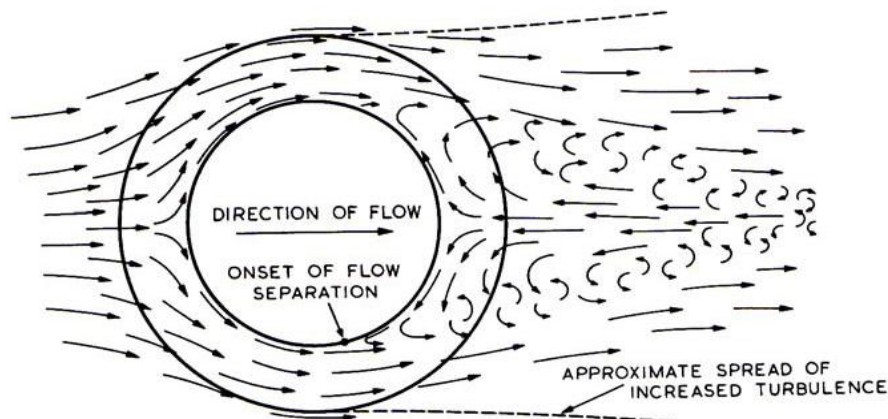


Figure 5. A schematic of general flow pattern over a second row of the staggered arrangement tube bundle [1]



As it was observed in Figure 4, the stream lines behind each tube row, inside the tube bank are approximately the same but different from the last row. For this reason, the velocity vector over the tube, only for third and fourth rows are shown in Figure 5(Left side). As it can be observed all models predict the separation angle from tube surface slightly after  $90^\circ$  which is in agreement with experimental results. Moreover, the velocity vector plots show a very good agreement in all methods. Interestingly, predicted velocity vector in a simple method such as Spalart-Allmaras (one-equation model) is in excellent agreement with more complicated models such as Transition SST model (four-equation model).

The other phenomenon connived in all experimental flow visualizations is flow separation from fin edge. Really it can not be observed in any experimental methods due to small fin thickness. The flow velocity vector over the fin edge is plotted on Figure 6(Right side). As it is clear, the onset of flow separation over fin occurs after  $120^\circ$ . So, flow separates sooner over the tube rather the fin. This, results in a very complicated flow around the tube inside the fin space. To show this complexity, the velocity vectors between two adjacent fins at plane  $\theta = 0^\circ$  (Windward) and  $\theta = 180^\circ$  (Leeward) for 4<sup>th</sup> row are shown in Figure 7. The horseshoe vortices are clear in this figure. Since the velocity vector from all models are schematically the same, the results of Transition SST model are shown for brevity's sake.

Flow temperature profile crossing tube bank has been shown in Figure 8. Since the flow is constrained inside the bank, temperature profile is also approximately the same for all models. However K- family is slightly different from the others. But behind the last row, the story is different and Spalart-Allmaras, k-kl- and Transition SST shows more agreement with each other and are slightly different from k- family. The same scenario is cast for the flow temperature profile crossing the fins, Figure 9.

## 5. Conclusions

In this paper, the effect of different turbulent models on simulating the flow passing over a four-row finned tube was studied. The selected  $Re$  Number is relatively low and the transient models are more reliable than fully turbulent models. The flow passing the circular fin is a complicated problem, not only due to geometry complexity, but also due to complexity in flow filed, flow separation, horseshoe vortices, generated wakes, etc; however, global performance of all models were acceptable.

Detailed study shows that the numerical solution may be used as a new tool to visualize flow passing a tube bundle. In spite of some discrepancy between results, it is still a reasonable method in comparison with the experimental methods. It is interesting that a simple model such as Spalart-Allmaras shows an acceptable performance and it may not be economical to use more complicated models. Additionally, in spite of acceptable performance of all models, results of k- family are somehow different from the others. However, since  $Re$  number is relatively low, the two new methods, K-Kl- and Transition SST show more compatibility with experimental correlations. Beside these two methods, SST k- model which is utilized to predict flow separation over smooth surface show also a very good compatibility with those two aforementioned methods.

The interesting observation is related to flow separation. The separation of flow passing over the tube occurs around  $\theta = 90^\circ$  while the separation on the fin edge occurs at  $\theta > 120^\circ$ . This phenomenon adds more complexity to the problem and also shows capability of numerical simulation as a flow visualization tool; because this observation can not be studied by experimental methods, due to very small fin thickness. Finally, from the temperature contours, it can be found out that more than 40% of fin area in leeward direction does not participate in heat transfer and the flow behind the fin is intact.

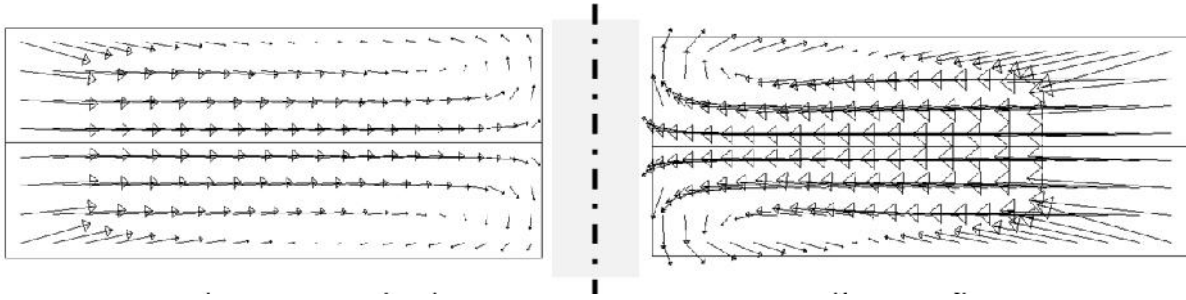


Figure 7. Velocity vector between two adjacent fins

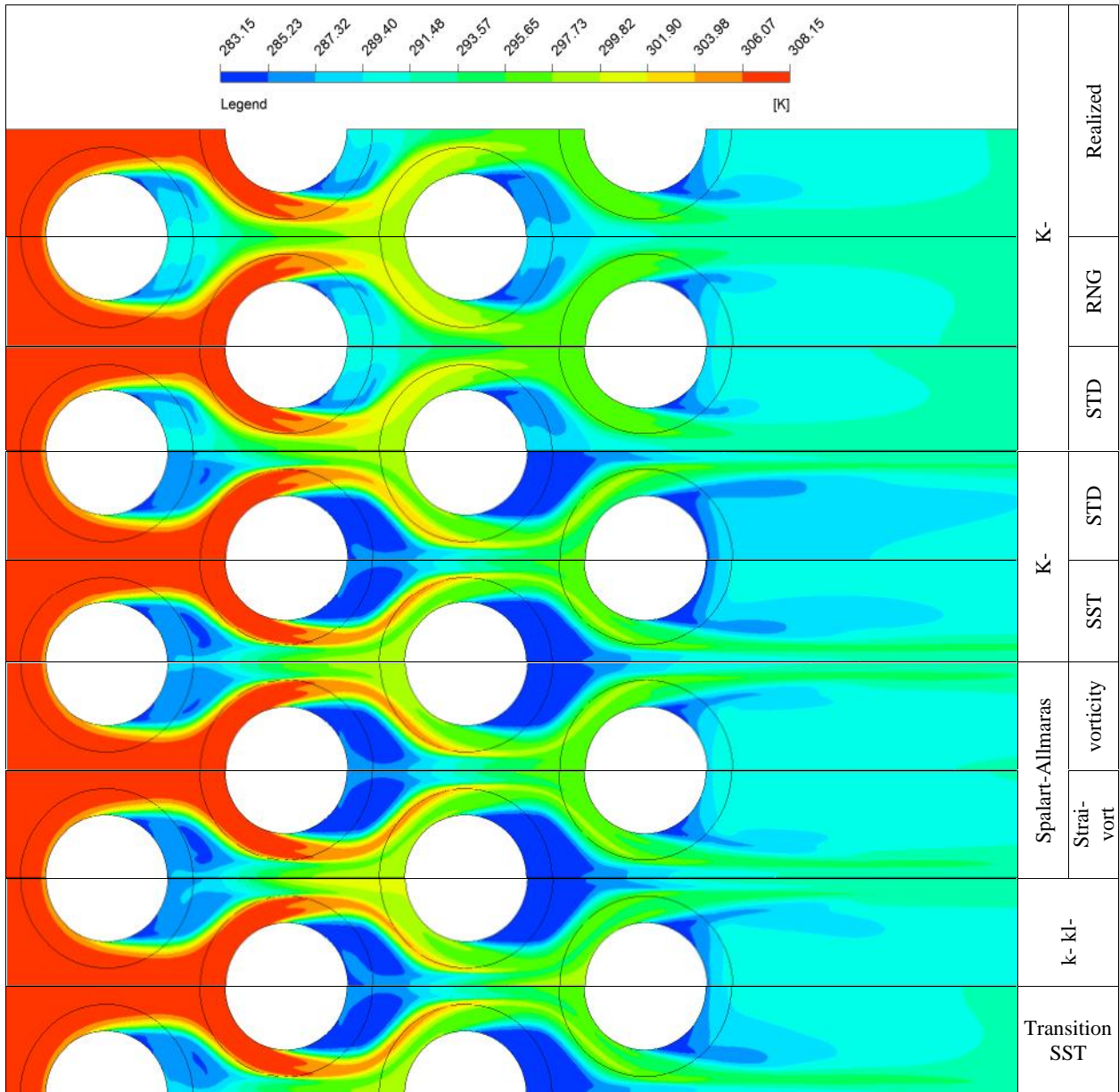


Figure 8. Flow temperature profile over tube in different models

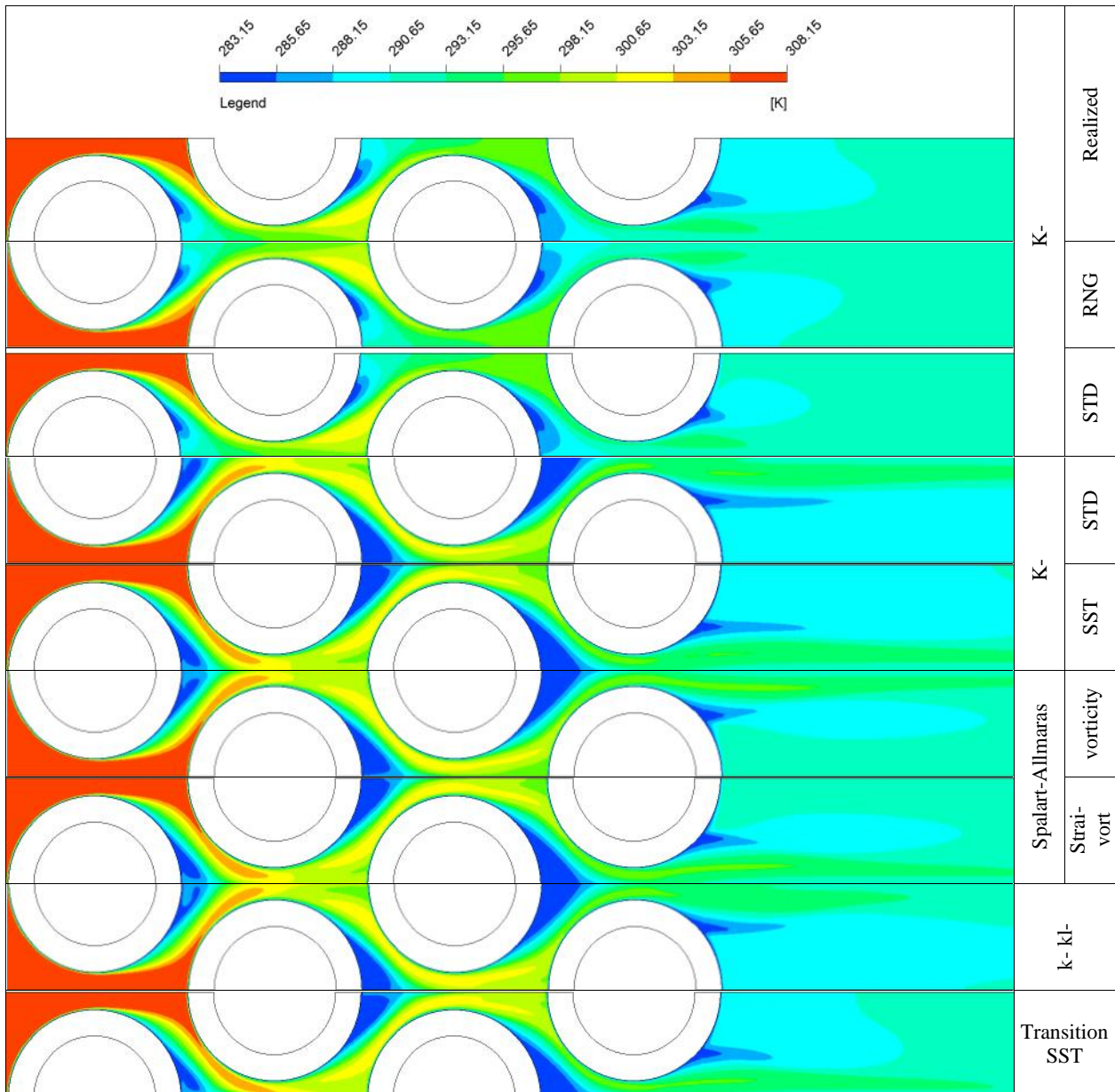


Figure 9. Flow temperature profile over Fins in different models

**Nomenclature**

$A = A_f + A_t$	Total fin tube area per unit length	$d_f$	Fin diameter
$A_f$	Fin surface area per unit length	$h$	Air side heat transfer coefficient
$A_t$	Tube surface area per unit length	$h_f$	Fin height
$Eu$	<i>Euler</i> number	$k$	Air thermal conductivity
$\dot{H}$	Air flow rate enthalpy	$k_f$	Fin thermal conductivity
$Nu$	<i>Nusselt</i> number	$s$	Fin spacing
$P$	Pressure	$t_f$	Fin thickness
$\dot{Q}$	Heat exchange	$u$	Air velocity
$S_l$	Longitudinal tube pitch	$u_{max}$	Maximum air velocity in tube bundle
$S_t$	Transverse tube pitch	$P$	Air pressure drop in bundle
$T_{in}$	Air inlet temperature	$\eta$	Fin efficiency
$T_{out}$	Air outlet temperature	$\Delta T_{lm}$	Log mean temperature difference
$T_w$	Tube wall temperature	$\mu$	Air viscosity
$d$	Tube outside diameter	$\rho$	Air density

## Reference

- [1] Neal, S.B.H.C. and J.A. Hitchcock, *A Study of the Heat Transfer Processes in Banks of Finned Tubes in Cross Flow, Using a Large Scale Model Technique*, Third International Heat Transfer Conference, Chicago, **3**(1966) , 290-298.
- [2] Legkiy, V.M., V.P. Pavlenko, Makarov, AS., and Zheludov, Y.A.S., *Investigation of Local Heat Transfer in a Tube with Annular Fins in Transverse Air Flow*, Heat Transfer Soviet Research, **6**(6) (1974), 101-107.
- [3] Stasiulevicius, J. and A. Skrinska, *Heat Transfer of Finned Tube Bundles in Cross flow*, Hemisphere Publishing, Washington, D.C (1988).
- [4] Hu X., *Local Heat and Mass Transfer Characteristics of Circular-Finned Tubes*, M.S. Thesis, The Johns Hopkins University, Baltimore, (1991).
- [5] Xi G.N. and K. Torikoshi, *Computation and Visualization of Flow and Heat Transfer in Finned Tube Heat Exchangers*, International Symposium on Heat Transfer, Tsinghua University, Beijing China, (7.10 - 11.10), 632-637, (1996).
- [6] Saboya, F.E.M. and E.M. Sparrow, *Local and average transfer coefficients for one-row plate fin and tube heat exchanger configuration*, ASME J. Heat Transfer, Ser. C **96** (3) (1974) 265-272.
- [7] Sheu, T.W.H. and S.F. Tsai, *A comparison study on fin surface in finned-tube heat exchangers*, Int. J. Numer. Meth. Heat Fluid flow **9** (1) (1999) 92–106.
- [8] Fiebig M., A. Gorse-Georgemann, Y. Chen, N.K. Mitra, *Conjugate heat transfer of a finned tube part A: Heat transfer behavior and occurrence of heat transfer reversal*, Numer. Heat Transfer, Part A **28** (1995) 133–146.
- [9] Romero-Mendez, R., M. Sen, K.T. Yang, R. McClain, *Effect of fin spacing on convection in a plate fin and tube heat exchanger*, Int. J. Heat Mass Transfer **43** (2000) 39–51.
- [10] Jang, J.Y., J.T. Lei, L.C. Liu, *The thermal-hydraulic characteristics of staggered annular finned-tube heat exchangers under dry and dehumidifying conditions*, Int. J. Heat Mass Transfer **41** (1998) 3321–3337.
- [11] Mon, M.S. and U. Gross, *Numerical study of fin-spacing effects in annular-finned tube heat exchangers*, Int. J. Heat Mass Transfer **47** (2004) 1953–1964.
- [12] Zhukauskas, A. A., *Investigation of Heat Transfer in Different Arrangements of Heat Exchanger Surfaces*, Teploenergetika, **21** (5) (1974), 40-46.
- [13] Jacobi, A.M. and R.K. Shah, *Air-side flow and heat transfer in compact heat exchangers: a discussion of enhancement mechanisms*, Heat Transfer Eng. **19** (4) (1998) 29–41.
- [14] FLUENT User Guide
- [15] Keith Walters, D. and D. Cokljat. "A three-equation eddy-viscosity model for Reynolds-averaged navier-stokes simulations of transitional flows". Journal of Fluids Engineering. 130. December (2008).
- [16] Schmidt, Th.E., *Der Wärmeübergang an Rippenrohre und die Berechnung von Rohrbündel-Wärmeaustauschern*, Kältetechnik, Band 15, Heft 12, (1963).
- [17] Verein Deutscher Ingenieure, VDI- Wärmeübergang, Berechnungsblätter für den Wärmeübergang, 8. Aufl. Berlin u.a., Springer, (2000).
- [18] Ward D. J. and E.H. Young, *Heat Transfer and Pressure Drop of Air in Forced Convection Across Triangular Pitch Banks of Finned Tubes*, Chemical Engineering Progress Symposium Series, **55** (29) (1959), 37-44.
- [19] Sparrow, E.M. and S.R. Chastain, *Effect of Angle of Attack on the Heat Transfer Coefficient for an Annular Fin*, Int. J. Heat Mass Transfer, **29** (1986), 1185-1191.
- [20] Watel, B.,S. Harmand and B. Desmet, *Influence of Flow Velocity and Fin Spacing on the Forced Convective Heat Transfer from an Annular-Finned Tube*, JSME international Journal, series B, **42** (1) (1999), 56-64.